# Effect of concurrent precipitation on recrystallization textures in commercial Al-Mn alloys

Tu Yiyou[1]　　Huang Linghui[1]　　Sun Zhongyue[1]　　Zhou Xuefeng[1]　　Jiang Jianqing[1,2]

([1] School of Materials Science and Engineering, Southeast University, Nanjing 211189, China)
([2] Nanjing University of Information Science and Technology, Nanjing 210044, China)

**Abstract:** The effect of concurrent precipitation on recrystallization textures in AA 3003 aluminum alloys was investigated using X-ray diffraction and electron backscattering diffraction(EBSD) analyses. A weak recrystallization texture was observed in the AA 3003 alloy annealed at 783 K due to the high annealing temperature. Under the same conditions, extremely high P $\{011\}\langle 111\rangle$ recrystallization textures were detected in the AA 3003 alloy added with 0.39% Sc. Based on the EBSD results, no intensely preferential orientation nucleation of recrystallization grains was observed in the early stage of recrystallization for both alloys. However, concurrent precipitation strongly retarded the growth of recrystallization grains, except for P nucleation sites, thereby conferring an apparent initial growth advantage for P nucleation sites compared with other nucleation sites. Therefore, a sharp P $\{011\}\langle 111\rangle$ texture appeared in concurrently precipitated AA 3003 alloys.

**Key words**：AA3003 alloy; concurrent precipitation; recrystallization texture

**doi**：10.3969/j.issn.1003−7985.2015.04.012

Recrystallization texture has been a subject of metallurgical research due to the fact that texture is one of the main factors responsible for the anisotropy of the mechanical properties of the final sheets[1−3]. The mechanisms of recrystallization textures in aluminum alloys are widely debated and generally interpreted using two theories[2,4−5]: 1) Oriented nucleation, in which the preferred formation of nuclei with special orientations determines the final recrystallization texture; and 2) Oriented growth, which originates from a random spectrum of nuclei and wherein structures with the optimal growth conditions dominate the recrystallization texture. However, discussion solely based on one of these two theories fails in most cases. Therefore, a combination of both theories has been proved to aid explanations of the recrystallization textures of aluminum alloys; this strategy is based on growth selection from a limited spectrum of preferentially formed nucleus orientations[2, 6−7].

The recrystallization texture of most aluminum alloys is characterized by a cubic orientation with scattering along the rolling direction toward the Goss orientation. As-deformed supersaturated AA 3000 series aluminum alloys conventionally result in different recrystallization textures after recrystallization annealing because of the effect of concurrent precipitation[6, 8−11]. Nes et al.[9] found that concurrent precipitation results in the formation of relatively strong P$\{011\}$ $\langle 455\rangle$ and ND-rotated cubic $\{001\}$ $\langle 310\rangle$ textures in commercial alloys. Moreover, continuous cast AA 3015 alloys exhibit remarkably strong recrystallization textures[10−11]. The formation of the P texture strongly depends on the annealing temperature[11−13]. However, the relationship between the concurrent precipitation and composition of recrystallization textures has been rarely reported in the literature. The present work aims to examine the effect of concurrent precipitation on the nucleation and growth of recrystallization grains at a high annealing temperature of 783 K in as-rolled commercial AA 3003 alloys and recrystallization texture components.

## 1　Materials and Experiments

We studied two Al alloy samples: 1) AA 3003: Al-0.93% Mn-0.45% Fe-0.08% Si-0.06% Cu-0.02% Ti and 2) AA 3003 + Sc: Al-0.90% Mn-0.39% Fe-0.10% Si-0.05% Cu-0.02% Ti-0.39% Sc (in mass fraction). The alloys were cast into 200 mm × 150 mm × 20 mm plates by using steel molds and then solution treated (ST) at 913 K for 72 h. The two types of ST plates were subsequently deformed into sheets by cold rolling with a true strain of 2.20. Finally, the rolled sheets were isothermally annealed at 783 K.

The microstructures of the cold rolled and annealed samples were observed through anodization and optical microscopy under polarized light. All the micrographs were obtained from longitudinal sections, defined by rolling direction (RD) and normal direction (ND).

The macro-texture measurements were performed using one-fourth thick cold-rolled sheets via X-ray diffraction

---

(XRD). The (111), (200), and (220) pole figures were measured up to a maximum tilt angle of 75° by the Schulz back-reflection method with Cu $K_\alpha$ radiation. Orientation distribution functions (ODFs) were calculated from incomplete pole figures by using a series expansion method[14]. These ODFs are presented as plots of constant $\varphi_2$ sections with isointensity contours in the Euler space, which is defined by Euler angles, namely, $\varphi_1$, $\Phi$, and $\varphi_2$. In addition, microtextures were monitored through electron backscatter diffraction (EBSD) analysis by using a field-emission scanning electron microscope (FEI Sirion).

## 2 Results and Discussion

### 2.1 Microstructure and texture of the as-rolled sheets

Fig. 1 shows the microstructures and textures of the as-rolled AA 3003 and AA 3003 + Sc alloys. Figs. 1(a) and (b) illustrate that both alloys display a fibrous microstructure, which is a typical deformation structure. Figs. 1(c) and (d) show that both the as-rolled alloys exhibit similar rolling texture, namely, copper {112} ⟨111⟩ textures, which is a typical rolling texture of aluminum alloys.
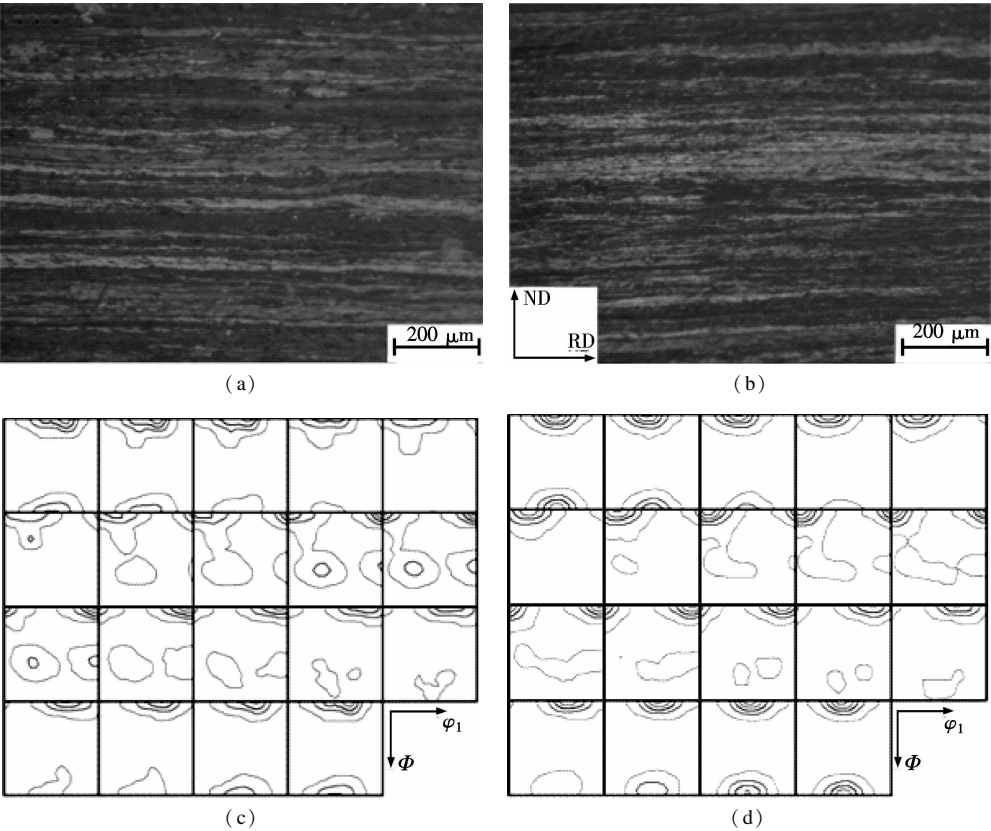


**Fig. 1** Microstructure and texture of the as-rolled alloys. (a) Microstructure of as-rolled AA 3003 alloy; (b) Microstructure of as-rolled AA 3003 + Sc alloy; (c) Texture of as-rolled AA 3003; (d) Texture of as-rolled AA 3003 + Sc alloy

### 2.2 Macro-recrystallization textures and recrystallization microstructures

Fig. 2 shows the recrystallization microstructures and macro-recrystallization texture of cold-rolled AA 3003 and AA 3003 + Sc alloys after annealing at 783 K. The AA 3003 alloy annealed at 783 K for 1 h was fully recrystallized, showing fine, equiaxed grains with a mean diameter of approximately 10 μm (see Fig. 2(a)). Recrystallization is not affected by the concurrent precipitation of Mn-bearing dispersoids. In principle, a high amount of stored deformation energy and a high density of microstructural heterogeneities for nucleation and precipitation are dispelled after recrystallization. This dispelling phenomenon tends to delay the precipitation of Mn-bearing dispersoids when the recrystallization occurs prior to precipitation. By contrast, the AA 3003 + Sc alloy displayed coarse and elongated recrystallization grains along the RD/ND plane (see Fig. 2(b)). The precipitation of Al₃Sc particles precedes the recrystallization in the as-rolled AA 3003 + Sc alloy annealed at 783 K. Moreover, the concurrent precipitation strongly affects the recrystallization behavior of the alloys due to the small nucleation barrier for the precipitation of Al₃Sc particles[15]. In addition, the Al₃Sc particles tend to precipitate at the grain boundaries, which are along the RD/TD plane in the deformed alloys. Consequently, the recrystallizing grains experience the highest drag in the direction normal to the rolling plane, leading to the pancake-like recrystallization of grains.

Recrystallization textures significantly differed between AA 3003 alloys with and without Sc addition. The precipitation of Mn-bearing precipitates starts after the recrystallization in the AA 3003 alloy because of the high annealing temperature of 783 K[15]. Consequently, the recrystallization textures are comprised of cubic {001} ⟨100⟩, weak ND-rotated {001} ⟨310⟩ and P {011} ⟨111⟩ components (see Fig. 2(c)). However, the recrystallization texture of the AA 3003 + Sc alloy shows an extremely sharp P {011} ⟨111⟩ component (see Fig. 2(d)), which is observed when the precipitation occurs prior to or simultaneously with recovery and recrystallization processes, i. e., concurrent precipitation[6].
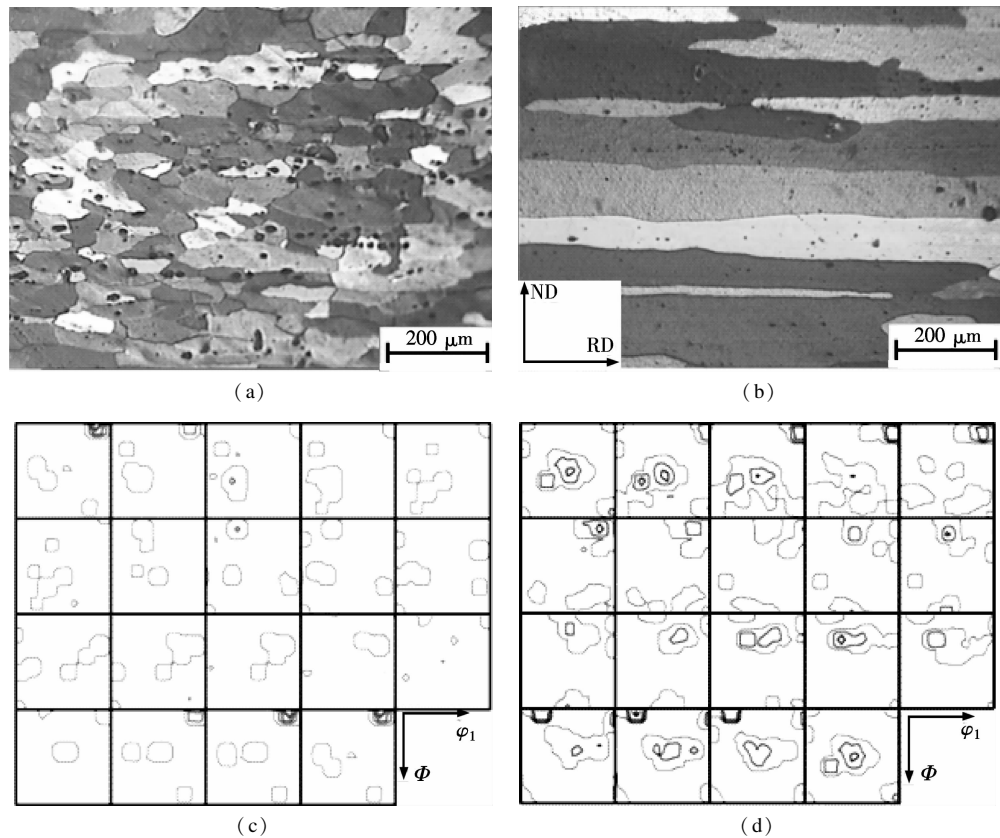


**Fig. 2** Recrystallization microstructures and macro-recrystallization textures of alloys after annealing at 783 K for 1 h. (a) Recrystallization microstructures of AA 3003 alloy; (b) Recrystallization microstructures of AA 3003 + Sc alloy; (c) Recrystallization textures of AA 3003 alloy; (d) Recrystallization textures of AA 3003 + Sc alloy

## 2.3　Micro-recrystallization textures

Fig. 3 demonstrates the EBSD maps and orientation relationships of the recrystallization grains of AA 3003 and AA 3003 + Sc alloys after annealing at 783 K. As shown in our previous work[15], the annealing temperatures are below the critical temperature $T_c$ of the alloy and recrystallization grains are expected to be large and pancakelike. However, in the present study, the EBSD maps show the presence of several fine, equiaxed recrystallization grains with numerous fractions of approximately 1/10 (see Fig. 3(a)). The crystallographic orientation of fine, equiaxed grains and large, pancake-like recrystallization grains are indicated by dash and solid lines, respectively, in the orientation relationship maps (see Fig. 3(b)). The orientation relationship maps demonstrate that most of the large, pancake-like grains are P- and ND-rotated cubic grains, which are indicated by solid lines, whereas the fine, equiaxed grains are randomly oriented and stop

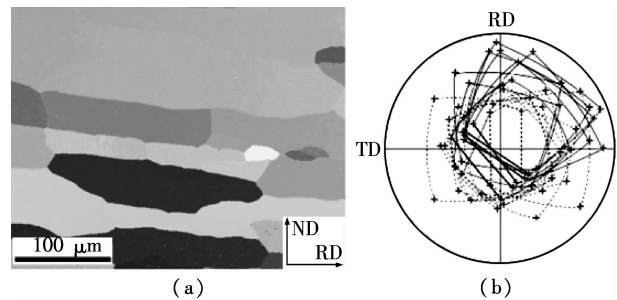growing after reaching an average size of approximately 15 μm.



**Fig. 3** EBSD maps of AA 3003 + Sc alloy after annealing at 783 K for 1 h. (a) EBSD orientation map; (b) Orientation relationship of grains in the (111) polar diagram

## 3　Discussions

The mechanisms of recrystallization textures in Al alloys are intensely debated and generally considered to

combine oriented nucleation and growth[2,4]. In the present work, a sharp P texture was observed in the AA 3003 + Sc alloy, whereas a weak texture was detected in the AA 3003 alloy. Considering the origin of P texture components, researchers must determine whether P oriented grains have a nucleation or growth advantage over other randomly oriented grains.

The EBSD maps show some nucleated recrystallization grains of AA 3003 (see Fig. 4(a)) and AA 3003 + Sc alloys (see Fig. 4(b)) at the beginning of recrystallization, i. e., annealing at 783 K. However, the nature of the nucleation sites of these orientations has not yet been fully identified. The nucleation of recrystallization in the AA3003 alloy occurs along the constituent particles, and the EBSD map shows that the recrystallization grains are randomly orientated with a mean diameter of approximately 10 μm (see Fig. 4(a)). Similarly, the number density of P- and ND-rotated cubic orientation grains shows the same order of magnitude as the randomly oriented grains in the AA 3003 + Sc alloys (marked by the arrows in Fig. 4(b)). However, the nucleated grains with P orientations are considerably larger than randomly oriented grains in the AA 3003 + Sc alloy. The volume fraction of P-oriented grains is higher than that of randomly oriented grains. Therefore, the sharp P texture appears at the beginning of recrystallization in the AA 3003 + Sc alloy.

Al$_3$Sc always occurs prior to recrystallization in the AA3003 alloy added with 0.4% Sc, and the concurrent precipitation remarkably affects the recrystallization (see Fig. 5). In the AA 3003 alloy, randomly oriented grains nucleate and grow uniformly. By contrast, the effective radii of grains with P- and ND-rotated cubic components typically develop to over 100 μm and are elongated in the RD/ND plane with an aspect ratio greater than 4.0. P nucleation sites have an initial growth advantage over other random nucleation sites because of their 40°-⟨111⟩ rotation relationship to the copper {112} ⟨111⟩ component[6]. The boundaries between such sites and the surrounding deformed matrix consist of 7-type interfaces and are minimally affected by precipitation and segregation. This situation results in precipitation-induced oriented growth. Moreover, precipitation tends to occur at the boundaries between the recrystallized deformation zones of random orientations and the copper deformation matrix, which present locally high supersaturation and low nucleation barriers. The large number of dense precipitates in the alloys provides sufficient Zener pinning and promptly terminates the growth of randomly oriented grains after nucleation. This phenomenon leads to the formation of fine, equiaxed recrystallization grains. Similarly, the P recrystallization texture in Al-Mn-Mg aluminum alloy is in excellent agreement with the oriented growth theory[5].





Fig. 5   TEM images showing the precipitation of a large number of Al$_3$Sc particles in the subgrains of the as-rolled AA3003 + Sc alloy annealed at 783 K for 500 s

## 4   Conclusion

In this study, the effect of concurrent precipitation on recrystallization textures in Al-Mn alloys was investigated. Concurrent precipitation strongly affected the recrystallization behavior of the alloys, leading to strong orientation densities close to the P {011} ⟨111⟩ recrystallization textures. However, no intensely preferential
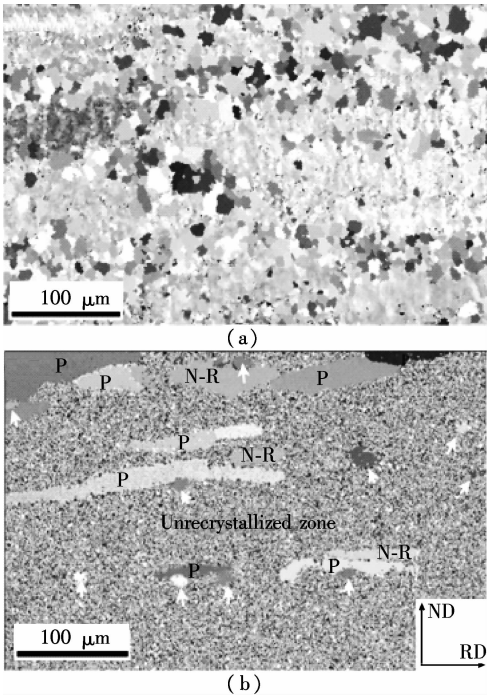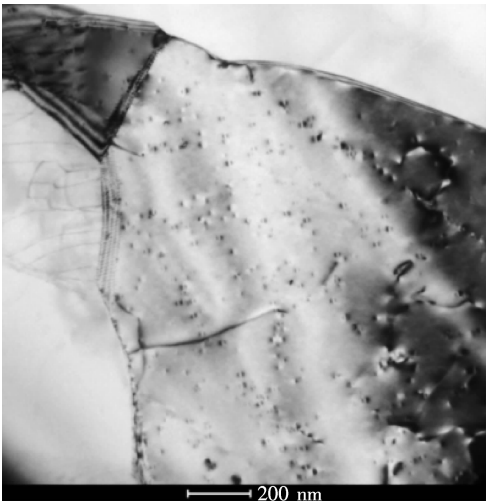
Fig. 4   Orientation of nucleated recrystallization grains at the beginning of recrystallization. (a) AA 3003 alloy annealed at 783 K for 25 s; (b) AA3003 + Sc alloy annealed at 783 K for 500 s

Recrystallization is completed before the beginning of significant precipitation in the as-rolled AA3003 alloy annealed at 783 K[15]. However, the precipitation of

orientation nucleation of recrystallization grains was observed. P nucleation sites show an evident initial growth advantage over other nucleation sites because of their 40°-⟨111⟩ rotation relationship to the copper {112} ⟨111⟩ component of the typical rolling textures of aluminum alloys. In addition, the sharp P {011} ⟨111⟩ texture appeared at the beginning of recrystallization.

## References

[1] Mishin O V, Jensen D J, Hansen N. Evolution of microstructure and texture during annealing of aluminum AA1050 cold rolled to high and ultrahigh strains [J]. *Metallurgical and Materials Transactions A*, 2010, **41** (11):2936-2948.

[2] Engler O, Yang P, Kong X W. On the formation of recrystallization textures in binary Al-1.3% Mn investigated by means of local texture analysis [J]. *Acta Materialia*, 1996, **44**(8):3349-3369.

[3] Mishin O V, Godfrey A, Jensen D J, et al. Recovery and recrystallization in commercial purity aluminum cold rolled to an ultrahigh strain [J]. *Acta Materialia*, 2013, **61**(14):5354-5364.

[4] Benum S, Nes E. Effect of precipitation on the evolution of cube recrystallisation texture [J]. *Acta Materialia*, 1997, **45**(11):4593-4602.

[5] Ma M, Wang W, Zhang J, et al. The role of oriented growth in p texture development in Al-Mn-Mg aluminum alloy [J]. *Journal of Material Engineering and Performance*, 2014, **23**(9):3257-3265.

[6] Tangen S, Sjolstad K, Furu T, et al. Effect of concurrent precipitation on recrystallization and evolution of the P-texture component in a commercial Al-Mn alloy [J]. *Metallurgical and Materials Transactions A*, 2010, **41** (11):2970-2983.

[7] Sidor J J, Decroos K, Petrov R H, et al. Evolution of recrystallization textures in particle containing Al alloys after various rolling reductions: experimental study and modeling [J]. *International Journal of Plasticity*, 2015, **66**(3):119-137.

[8] Liu W C, Morris J G. Recrystallization textures of the M{113}⟨110⟩ and P{011}⟨455⟩ orientations in a supersaturated Al-Mn alloy [J]. *Scripta Materialia*, 2007, **56**(3):217-220.

[9] Daaland O, Nes E. Recrystallization texture development in commercial Al-Mn-Mg alloys [J]. *Acta Materialia*, 1996, **44**(4):1413-1435.

[10] Liu W C, Morris J G. Comparison of the texture evolution in cold rolled DC and SC AA 5182 aluminum alloys [J]. *Materials Science and Engineering A*, 2003, **339** (1/2):183-193.

[11] Liu W C, Morris J G. Evolution of recrystallization and recrystallization texture in continuous-cast AA 3015 aluminum alloy [J]. *Metallurgical and Materials Transactions A*, 2005, **36**(10):2829-2848.

[12] Huang K, Engler O, Li Y J, et al. Evolution in microstructure and properties during non-isothermal annealing of a cold-rolled Al-Mn-Fe-Si alloy with different microchemistry states [J]. *Materials Science and Engineering A*, 2015, **628**(3):216-229.

[13] Liu W, Ma M, Yang F. Effect of the heat treatment on the cube recrystallization texture of Al-Mn-Mg aluminum alloy [J]. *Metallurgical and Materials Transactions A*, 2013, **44**(6):2857-2868.

[14] Bunge H J. *Texture analysis in materials science: mathematical methods* [M]. Butterworths, 1982.

[15] Tu Y, Qian H, Zhou X, et al. Effect of scandium on the interaction of concurrent precipitation and recrystallization in commercial AA3003 aluminum alloy [J]. *Metallurgical and Materials Transactions A*, 2014, **45** (4):1883-1891.

# 并发沉淀析出对 Al-Mn 变形铝合金再结晶织构的影响

涂益友[1]　　黄羚惠[1]　　孙中岳[1]　　周雪峰[1]　　蒋建清[1,2]

([1] 东南大学材料科学与工程学院,南京 211189)
([2] 南京信息工程大学,南京 210044)

**摘要:**采用 X 射线衍射和电子背散射衍射研究了第二相析出对冷轧 AA3003 铝合金再结晶织构的影响.当退火温度为 783 K 时,由于退火温度高,AA3003 合金再结晶织构不明显.而在相同退火条件下,在添加了 0.39% 钪的 AA3003 合金中发现了强烈的 P {011} ⟨111⟩织构.采用 EBSD 分析再结晶初期的合金,发现 2 种合金的再结晶形核均无明显择优取向.第二相颗粒析出先于或与再结晶同时发生时,会显著阻碍除 P 取向晶核之外的再结晶晶核的长大,导致 P 取向的再结晶晶核长大速度明显快于其他取向的晶核.因此,在并发沉淀析出影响的 AA3003 合金中形成了强烈的 P{011}⟨111⟩再结晶织构.

**关键词:**AA3003 合金;并发沉淀析出;再结晶织构

**中图分类号:**TG113.12